CFTR-deficient pigs display peripheral nervous system defects at birth

Leah R. Reznikov[a], Qian Dong[b], Jeng-Haur Chen[a,c], Thomas O. Moninger[d], Jung Min Park[a], Yuzhou Zhang[e], Jianyang Du[a,c], Michael S. Hildebrand[e], Richard J. H. Smith[e], Christoph O. Randak[b], David A. Stoltz[a], and Michael J. Welsh[a,c,f,1]

Departments of [a]Internal Medicine, [b]Pediatrics, [e]Otolaryngology, [d]Central Microscopy Research Facility, and [f]Molecular Physiology and Biophysics, [c]Howard Hughes Medical Institute, University of Iowa Roy J. and Lucille A. Carver College of Medicine, Iowa City, IA 52242

Contributed by Michael J. Welsh, December 27, 2012 (sent for review November 23, 2012)

Peripheral nervous system abnormalities, including neuropathy, have been reported in people with cystic fibrosis. These abnormalities have largely been attributed to secondary manifestations of the disease. We tested the hypothesis that disruption of the *cystic fibrosis transmembrane conductance regulator* (*CFTR*) gene directly influences nervous system function by studying newborn *CFTR*$^{-/-}$ pigs. We discovered CFTR expression and activity in Schwann cells, and loss of CFTR caused ultrastructural myelin sheath abnormalities similar to those in known neuropathies. Consistent with neuropathic changes, we found increased transcripts for *myelin protein zero*, a gene that, when mutated, can cause axonal and/or demyelinating neuropathy. In addition, axon density was reduced and conduction velocities of the trigeminal and sciatic nerves were decreased. Moreover, in vivo auditory brainstem evoked potentials revealed delayed conduction of the vestibulocochlear nerve. Our data suggest that loss of *CFTR* directly alters Schwann cell function and that some nervous system defects in people with cystic fibrosis are likely primary.

Mutations in the *cystic fibrosis transmembrane conductance regulator* (*CFTR*) gene cause cystic fibrosis (CF), a common, life-shortening, autosomal recessive disease (1–3). CFTR is an anion channel that is expressed in many epithelial organs where its loss causes exocrine pancreatic destruction, airway disease with infection and inflammation, and intestinal obstruction with meconium ileus.

In addition to disease in epithelial organs, several studies have reported that people with CF have peripheral nervous system abnormalities. For example, peripheral neuropathy, including decreased nerve conduction velocity, has been described in people with CF, a finding that could not be attributed to duration of disease, sex, age, or body mass index (4, 5). Decreased innervation of sweat gland acini and ducts in people with CF has also been reported (6). Gastric myoelectrical activity is impaired in CF, suggesting possible altered nerve function (7). Reports also suggest abnormal cholinergic and adrenergic sensitivity in pupillary constriction, sweat and saliva secretion, blood pressure regulation, and bronchoconstriction in people with CF (8, 9). Several other studies have reported abnormal neural function in CF (10–14). The interpretation of these multiple observations has been confounded by possible malnutrition, chronic illness, and drug administration, and thus it has been difficult to distinguish nervous system abnormalities that are directly caused by loss of CFTR from those that might be secondary. However, two observations have suggested that loss of CFTR might have direct effects on nervous system function. First, *CFTR* mRNA and/or protein have been detected in multiple regions of the nervous system in mice, rats, rabbits, cows, and humans (15–18). Although many of those studies lacked a null control, they suggested that *CFTR* is expressed in the nervous system. Second, some nervous system abnormalities reported in people with CF have also been detected in people heterozygous for *CFTR* gene mutations (9, 13, 19). Because carriers of *CFTR* mutations lack classic manifestations of CF, these observations suggest a direct functional effect of CFTR loss.

Studies of nervous system abnormalities in CF have been limited because it is not possible to study humans, i.e., infants with CF, in the absence of potential malnutrition, chronic disease, and various treatments. Moreover, the field has lacked an animal model that develops typical manifestations of CF. To circumvent these obstacles, we recently disrupted the *CFTR* gene in pigs to generate a porcine model of CF (20, 21). At birth, *CFTR*$^{-/-}$ pigs display intestinal lesions (meconium ileus and microcolon), exocrine pancreatic destruction, and gallbladder abnormalities. The airways and lungs of newborn *CFTR*$^{-/-}$ pigs lack infection and inflammation, but display a bacterial host defense defect (22). Over the ensuing weeks and months after birth, these pigs spontaneously develop lung disease. These abnormalities are remarkably similar to those in people with CF. Thus, using this model we tested the hypothesis that CFTR is expressed in the nervous system and that loss of CFTR directly affects nervous system function.

Results

CFTR Is Expressed in the Peripheral and Central Nervous Systems of Newborn Pigs. To test whether the newborn pig nervous system expresses *CFTR*, we isolated RNA and performed RT-PCR from the maxillary branch of trigeminal and optic nerves, which allowed us to sample areas enriched in glial cells and axons, and from the trigeminal ganglion and the cerebellum, which provided regions enriched in neurons. In all cases, we detected *CFTR* transcripts (Fig. S1*A*).

Using the trigeminal nerve as a model system, we next asked how much *CFTR* was present compared with traditional airway epithelia. Quantitative RT-PCR (qRT-PCR) indicated that there was substantially less in the nerve compared with airway epithelia (Fig. S1*B*). Undeterred by this, we also examined sagittal sections of the trigeminal nerve by immunocytochemistry to test for CFTR protein. CFTR immunostaining varied from diffuse to punctate, and staining intensity varied in different sections (Fig. 1). However, we detected no CFTR immunostaining in any of the *CFTR*$^{-/-}$ sections (Fig. 1*B* and Fig. S2). CFTR immunostaining did not colocalize with β-tubulin III, a marker of axons, or fluoromyelin, which labels the myelin sheath of axons (Fig. 1 *A* and *C*). Instead, CFTR appeared to be present in Schwann cells,

Author contributions: L.R.R., Q.D., J.-H.C., Y.Z., J.D., M.S.H., R.J.H.S., C.O.R., D.A.S., and M.J.W. designed research; L.R.R., Q.D., J.-H.C., T.O.M., J.M.P., Y.Z., and M.S.H. performed research; L.R.R., Q.D., J.-H.C., J.M.P., C.O.R., and M.J.W. analyzed data; and L.R.R. and M.J.W. wrote the paper.

Conflict of interest statement: M.J.W. was a co-founder of Exemplar Genetics, a company to house and produce porcine models of human diseases. M.J.W. holds less than 3% equity and does not receive any money for services.

Freely available online through the PNAS open access option.

[1]To whom correspondence should be addressed. E-mail: michael-welsh@uiowa.edu.

This article contains supporting information online at www.pnas.org/lookup/suppl/doi:10.1073/pnas.1222729110/-/DCSupplemental.

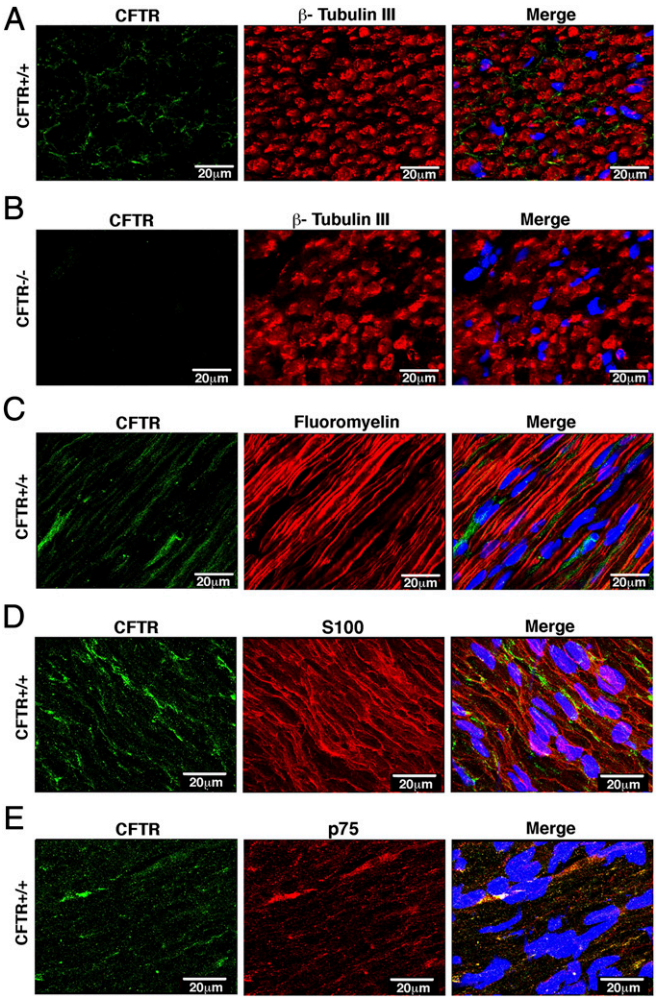

Fig. 1. CFTR is expressed in trigeminal nerve Schwann cells. Data are confocal microscopic images of trigeminal nerve immunostained for CFTR (green) and marker indicated above middle panels (red). Nuclei were stained with DAPI (blue). (*A*) Transverse cross-section with axons stained with β-tubulin III antibody. (*B*) $CFTR^{-/-}$ trigeminal nerves immunostained for CFTR and β-tubulin III. Other controls in $CFTR^{-/-}$ nerves are in Fig. S2. (*C*) Sagittal cross-section immunostained with fluoromyelin. (*D*) Section stained with S100 antibody, a marker of Schwann cells. (*E*) Section stained with p75 antibody, also a marker of Schwann cells. (Scale bar, 20 μm.)

as determined by colocalization with Schwann cell markers S100 and p75 (Fig. 1 *D* and *E*).

To further confirm CFTR expression in Schwann cells, we isolated and cultured porcine Schwann cells (Fig. 2*A*). We attempted to identify CFTR by immunocytochemistry, but nonspecific staining in cultured $CFTR^{-/-}$ Schwann cells made specific detection problematic. Therefore, we used whole-cell patch-clamp recordings to test for CFTR activity (Fig. 2*B*). $CFTR^{+/+}$ Schwann cells had protein kinase A (PKA) and ATP-mediated Cl^- currents that were not voltage-activated and were inhibited by GlyH-101, an inhibitor of CFTR (23). $CFTR^{-/-}$ Schwann cells showed negligible current.

Loss of CFTR Alters Myelin Sheath Structure and Myelin Gene Expression. Identification of CFTR in Schwann cells suggested that myelination might be affected upon loss of CFTR. Therefore, we used electron microscopy to assess myelin sheath structure in the trigeminal nerve. Many $CFTR^{-/-}$ axons exhibited a "ringed" appearance characterized by dark inner and outer bands (Fig. 3*C*). More interestingly, we also observed myelin infoldings (Fig. 3 *D* and *E*), a feature of Charcot–Marie–Tooth disease (24–27). The similarities between the myelin structure of nerves isolated from $CFTR^{-/-}$ pigs and the nerves of Charcot–Marie–Tooth disease suggested that perhaps other similarities also existed. Therefore, because mutations in myelin genes cause Charcot–Marie–Tooth disease (28), we hypothesized that myelin gene expression might be affected by loss of *CFTR*. We focused on myelin protein zero (MPZ), a major constituent of peripheral myelin, the loss or gain of function of which causes Charcot–Marie–Tooth disease (29–31). qRT-PCR revealed an increase in *MPZ* mRNA in trigeminal nerves of newborn $CFTR^{-/-}$ pigs (Fig. 4*A*). In previous studies, an increase in *MPZ* transcripts was accompanied by changes in transcripts for myelin basic protein (*MBP*), a minor structural component of peripheral myelin (32, 33). Indeed, *MBP* mRNA was also increased in $CFTR^{-/-}$ trigeminal nerves (Fig. 4*B*). To test whether the differences in *MPZ* and *MBP* reflected a global change in Schwann cell gene expression, we also assayed transcripts for *connexin 32* (*CNX32*), a gap junction protein, and for *annexin 2* (*ANX2*), a protein increased following nerve injury (34), and found no differences.

Axon Density Is Reduced in $CFTR^{-/-}$ Pigs. Changes in *MPZ* gene dosage can cause axonal (axon loss), demyelinating (loss of myelin), or intermediary types of Charcot–Marie–Tooth disease (29, 35, 36). Therefore, we hypothesized that axon density might also be affected in CF pigs. We measured myelinated axon density (number of axons/μm^2) in the maxillary branch of the trigeminal nerve and discovered that both $CFTR^{-/-}$ and $CFTR^{+/-}$ pigs had reduced density (Fig. 5*A* and Fig. S3). The trigeminal nerve circumference did not differ across genotypes (Fig. 5*B*), suggesting that reduced axon density represented a loss of axons.

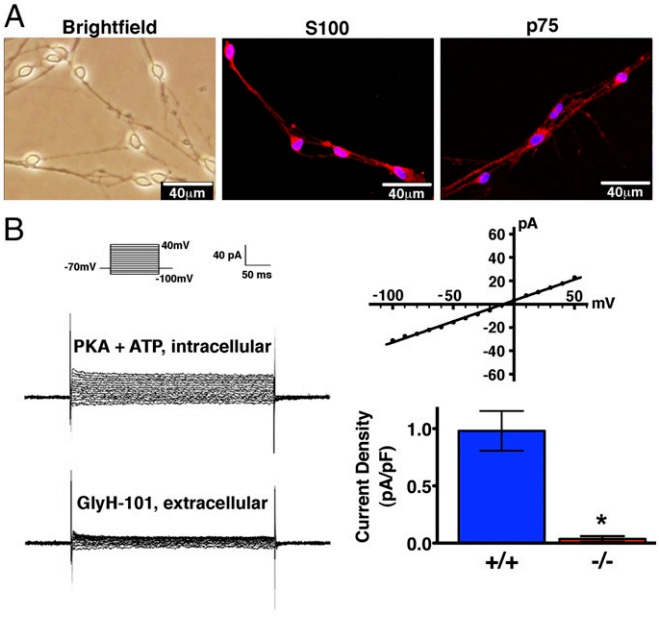

Fig. 2. CFTR is functionally active in Schwann cells. (*A*) Primary cultures of porcine Schwann cells were used 4 wk after seeding when they had developed the specific bipolar morphology and a phase-bright cell body under differential interference contrast microscopy. Schwann cells were positive for the phenotypic markers S100 and p75. (*B*) Whole-cell current recorded in the presence of PKA and ATP in the pipette solution and 1 min after adding 100 μM of CFTR inhibitor GlyH-101 to the bath solution. (*Left*) Example of currents from one cell; *Inset* shows voltage-pulse protocol. (*Upper Right*) Example of current-voltage relationship. (*Lower Right*) Data from five $CFTR^{+/+}$ Schwann cells and seven $CFTR^{-/-}$ Schwann cells. *$P = 0.003$ (Mann–Whitney rank sum test).

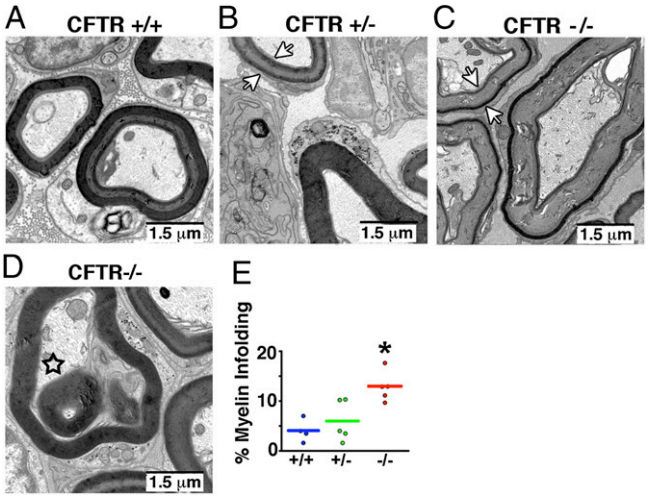

Fig. 3. Loss of *CFTR* alters myelin sheath structure. Images are transmission electron photomicrographs of myelin sheath in trigeminal nerve of $CFTR^{+/+}$ (*A*), $CFTR^{+/-}$ (*B*), and $CFTR^{-/-}$ (*C* and *D*) pigs. Arrows in *B* and *C* point to the ringed appearance of the myelin sheath. Star in *D* indicates myelin infolding. Myelin infoldings (*E*) were observed in a greater percentage of CF axons. n = 385 axons total from four $CFTR^{+/+}$ pigs; n = 404 axons total from four $CFTR^{+/-}$ pigs; and n = 602 axons total from four $CFTR^{-/-}$ pigs. (Scale bars, 1.5 μm.)

We also noted that small myelinated axons composed a smaller portion of the total population of axons in $CFTR^{-/-}$ pigs (Fig. 5*E*). This was further evidenced in average diameter measurements and curve-fitting analysis, in which a shift toward a greater diameter was observed (Fig. 5 *C*–*G*).

Loss of CFTR Reduces Nerve Conduction Velocity in Situ and in Vivo. The multiple similarities between $CFTR^{-/-}$ pig nerves and nerves in Charcot–Marie–Tooth disease, including changes in myelin sheath structure, *MPZ* expression, and axon loss, predicted that nerve conduction velocity might also be affected. We found that the maxillary branch of $CFTR^{-/-}$ trigeminal nerves showed a small but significant reduction in conduction velocity (Fig. 6*A* and Table S1). The sciatic nerve, which is composed of sensory and motor axons, also displayed a strong trend for reduced conduction velocity (Fig. 6*B* and Table S1).

As a test of in vivo nerve function, we measured auditory brainstem evoked potentials. We discovered that waves I and II, but not III and V, were delayed in $CFTR^{-/-}$ pigs (Fig. 6 *C* and *D* and Table S2). A delay in waves I and II could be due to either impaired air or nerve conduction. However, the wave I–II interval was also mildly prolonged (Fig. 6*E*), suggesting reduced conduction velocity in the vestibulocochlear nerve (37). Other intervals and peak-to-peak amplitudes were not affected (Table S2).

Discussion

Although it is well known that CFTR is expressed in epithelia (1), it has been suggested that CFTR is also present in the nervous system (15–18). Our data not only confirm this, but also suggest that Schwann cells are an important site of expression. Surprisingly, we discovered that loss of *CFTR* caused changes in nerves similar to those observed in Charcot–Marie–Tooth disease. These similarities included the following: (*i*) myelin sheath abnormalities (25–27); (*ii*) increased *MPZ* transcripts (29, 32, 33, 38, 39); (*iii*) reduced axon density (40, 41); and (*iv*) slowed nerve conduction velocity.

Newborn CF pigs displayed features of both axonal and demyelinating neuropathy, a finding congruent with previous studies describing axonal and/or demyelinating neuropathy in people with CF (4, 5, 42). For example, we observed a reduction in nerve conduction velocity, with no effect on amplitude, and increased incidence of myelin infoldings, consistent with a demyelinating neuropathy (24, 40). However, the defect in conduction velocity was minor, and there was no thinning of the myelin sheath, but there was a loss of small myelinated axons, consistent with an axonal neuropathy. This intermediary phenotype is likely due to the mild increase in *MPZ* mRNA (43, 44). For example, the threshold for dysmyelination (failure of Schwann cell differentiation and myelin formation) induced by overexpression of *MPZ* is between 30 and 80% overexpression (33). Thus, perhaps the 40% increase in *MPZ* expression caused a dysmyelination phenotype, in which loss of axons and reduced conduction velocity can be observed (45, 46).

How might loss of CFTR in Schwann cells cause these changes? Cl^- channels in Schwann cells are thought to stabilize membrane potential (47); therefore, removal of a Cl^- channel might destabilize membrane potential and cause changes in ion flux to be exaggerated. Indeed, exaggerated purinergic-mediated Ca^{2+} influx in Schwann cells has been associated with increased myelin gene expression and is a proposed pathogenic mechanism in Charcot–Marie–Tooth disease (32). Additionally, previous studies have shown that disruption of the *potassium-chloride cotransporter 3* (*KCC3*), a gene expressed in peripheral nerves, Schwann cells, and neurons, causes periaxonal fluid accumulation, increased myelinated axon diameter, reduced axon number, and peripheral neuropathy in mice and humans (48). Thus, our data are consistent with an important role for Cl^- transport in Schwann cells.

As outlined in the Introduction, many reports have described altered nervous system function in people with CF (4–14). Our results may provide an explanation for some of those abnormalities by indicating that altered Schwann cell function, and hence neuronal function, can occur as a primary defect independent of the secondary consequences of the disease. People who are heterozygous for CF mutations have a neurophysiological phenotype intermediate between non-CF and CF (9, 13, 19). In several, although not all cases, our data indicate that $CFTR^{+/-}$ pigs also manifest an intermediate phenotype. These observations open the door for speculation. On one hand, might *CFTR* heterozygosity have a negative consequence for carriers? On the other hand, it has long been speculated that carriers of a CF-associated mutation have a selective advantage that favors expansion of CF

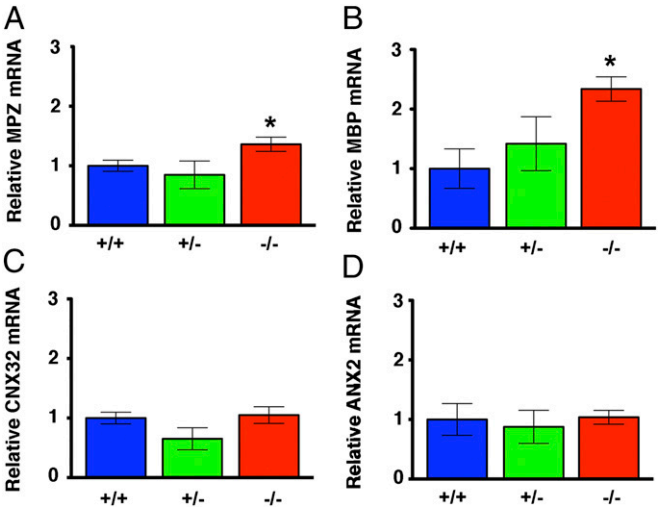

Fig. 4. Myelin gene transcripts are altered in trigeminal nerve of newborn $CFTR^{-/-}$ pigs. Data are qRT-PCR for transcripts of *MPZ* (*A*), *MBP* (*B*), *CNX32* (*C*), and *ANX2* (*D*). For $CFTR^{+/+}$, n = 5 animals; $CFTR^{+/-}$, n = 4 animals; $CFTR^{-/-}$, n = 6 animals. Data are expressed relative to average $CFTR^{+/+}$ levels. *P < 0.05 compared with $CFTR^{+/+}$.

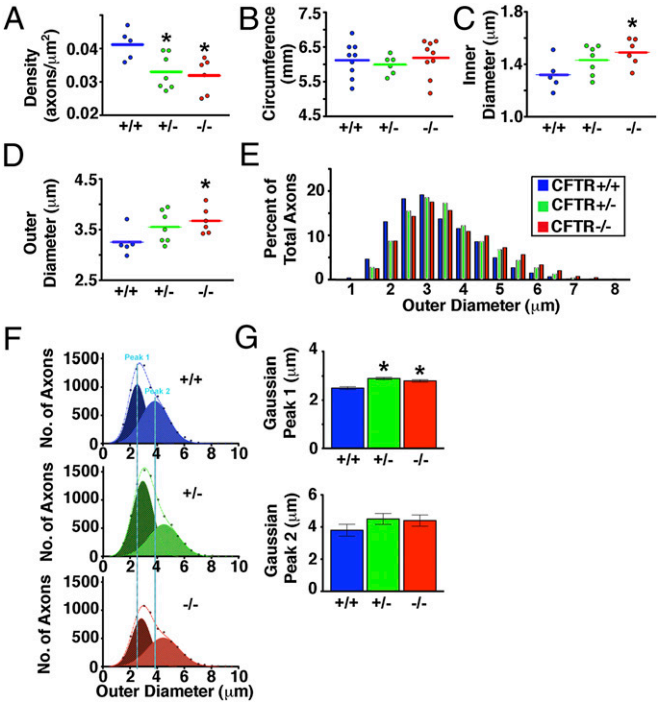

Fig. 5. Lack of *CFTR* decreases axon density and increases axon diameter in the trigeminal nerve. Data are from five $CFTR^{+/+}$ newborn pigs (7,210 total myelinated axons), seven $CFTR^{+/-}$ newborn pigs (8,229 total myelinated axons), and six $CFTR^{-/-}$ newborn pigs (6,127 total myelinated axons). In *A–D*, each point represents data from an individual animal (800–1,500 axons per animal). *$P < 0.05$ compared with $CFTR^{+/+}$. (*A*) Axon density. (*B*) Trigeminal nerve circumference. (*C*) Inner diameter or axonal diameter. (*D*) Outer diameter (the axon plus the myelin sheath). (*E*) Distribution of outer diameters as a percentage of total axons. (*F*) Curve fitting of the outer diameter of two main populations of myelinated axons. Dashed lines are the total populations, and the two curves are Gaussian peaks (labeled peak 1 and peak 2). Vertical blue lines highlight peaks in $CFTR^{+/+}$ newborn pigs. (*G*) Peaks from Gaussian curve fitting.

mutations in the population. Perhaps a neurological phenotype might provide an advantage to *CFTR* heterozygotes, although what that advantage might be remains unknown.

Our study has advantages and limitations. First, we used an animal model that recapitulates human CF (21, 22). Second, the nervous system of the pig is more similar to that of the human than is the mouse's nervous system (49). Third, by studying newborn pigs, we were able to eliminate secondary consequences of disease. Fourth, we used multiple assays to test the consequences for *CFTR* loss. A limitation of our study is that our data do not address the role of neuronal CFTR, and therefore we are not able to exclude the possibility that *CFTR* in neurons contributes to the phenotypes that we observed. For example, Cl^- channels in neurons are often inhibitory; thus, it is possible that neuronal CFTR might protect against excitotoxicity and that loss of CFTR consequently negatively impacts neurons. Additional studies will be required to fully dissect the role of CFTR in neurons versus Schwann cells and other glia.

Loss of *CFTR* in epithelia causes disease. However, might altered neural function contribute to or modulate disease in people with CF? Our data cannot answer that question, but we speculate that it might in several ways. Increasing evidence suggests a role for the nervous system in modulating inflammation; for example, vagal nerve activity dampens inflammation (50). Several previous reports have suggested that there is an overly exuberant inflammatory response to airway infections in patients with CF (51), and we wonder if impaired nervous system function might contribute to that. Neural activity also regulates submucosal gland secretion (52) and intestinal motility (53, 54). Although loss of CFTR in these epithelial tissues is undoubtedly the key factor in CF disease, it is interesting to speculate that altered neuronal function might contribute to mucus secretion from airway submucosal glands (52), the intestinal obstruction of meconium ileus in newborns (1), and/or the distal intestinal obstruction syndrome in older patients with CF (1, 55).

Materials and Methods

Animals. We previously reported generation of $CFTR^{+/-}$ and $CFTR^{-/-}$ pigs (21, 22). Animals were mated, and progeny were studied as previously described. Newborn male pigs were studied less than 24 h after birth. Piglets were weighed, sedated with ketamine and xylazine, and euthanized with an i.v. overdose of pentobarbital/phenytoin. All animal experiments were approved by the University of Iowa Institutional Animal Care and Use Committee.

RT-PCR. Brain tissues and cultured cells were rapidly removed/harvested and placed immediately on dry ice. Total RNA was isolated with the Qiagen Lipid Tissue RNeasy kit per the manufacturer's directions. RNA quality and concentration were assessed via Nanodrop and Agilent Technology. RNA was reverse-transcribed with the SuperScript III First Strand Synthesis Kit (Invitrogen). The following primer sequences were used: actin (forward, 5′-CTGCGGCATCCACGAAACT-3′; reverse, 5′-GTGATCTCCTTCTGCATCCTGTC-3′); CFTR (forward, 5′-CTGGAGCCTTCAGAGGGTAAAAT-3′; reverse, 5′-AGTTGGCACGCTTTGATGACACTCC-3′); myelin protein zero (forward, 5′-CTGCAGAGGAGGCTCAGTGCCA-3′; reverse, 5′-TCCTTGCGAGACTCCCCCAACC-3′); myelin basic protein (forward, 5′-CATGGACCACGCCAGGCACGGCTT-3′; reverse, 5′-CGCGTGGTGTCCATCCTTGCCCGAG-3′); annexin 2 (forward, 5′-TGCATTTGGGGACGCTCGCA-3′; reverse, 5′-GGTGACCTCGTCCACACCTTTGG-3′); connexin 32 (forward, 5′-AGGCGCTCCCCAAGGTGTGAATGAG-3′; reverse, 5′-CGTAGCAGACGCTGTTGCAGCC-3′). Primer efficiency and validation were performed as described (56). PCR was performed in sample triplicates with RT^2 SYBR Green qPCR Master Mixes (SA Biosciences) and a 7500 Fast Real-Time PCR System (Applied Biosystems), following the manufacturers' protocol. RNA that was not reverse-transcribed was used as control. Standard ΔΔCT method with actin as a reference gene was used for analysis. For end-point PCR studies, amplification of *CFTR* was accomplished using the above primers and AccuPrime SuperMix II (Invitrogen). Parameters were as follows: 30 cycles at 94 °C for 30 s, 55 °C for 30 s, and 68 °C for 1 min, with a final extension cycle of 68 °C for 7 min. Products were separated on a 1.5% agarose gel and visualized using a BioChemi system.

Schwann Cell Cultures. Schwann cells were cultured using methods similar to those previously described (57). Briefly, trigeminal nerves were removed from newborn pigs, chopped into small pieces, and digested in 3 mL of 3 mg/mL

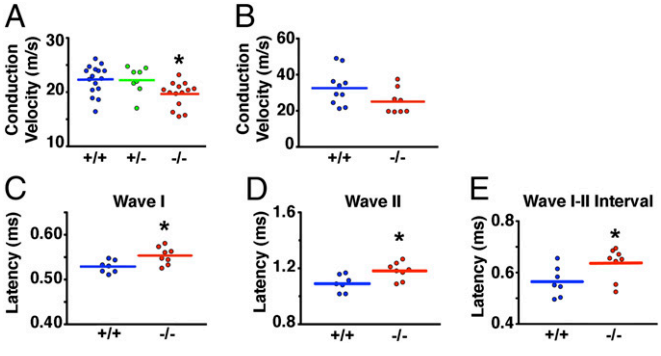

Fig. 6. Conduction velocity is reduced in the trigeminal, sciatic, and vestibulocochlear nerves of newborn $CFTR^{-/-}$ pigs. Trigeminal nerve showed reduced conduction velocity (*A*) whereas the sciatic nerve (*B*) showed a strong trend for reduced conduction velocity ($P = 0.084$). The compound action potential amplitude and the area under the curve are shown in Table S1. (*C–E*) Latencies of wave I and wave II and the wave I–wave II interval of in vivo auditory brainstem responses. Latency of other waves and other intervals did not differ between $CFTR^{+/+}$ and $CFTR^{-/-}$ pigs (Table S2). *$P < 0.05$ compared with $CFTR^{+/+}$. Each point represents the data collected from an individual animal.

collagenase/0.25% trypsin for 30 mins at 37 °C. Enzymes were inhibited by added 10% (vol/vol) FCS, and digested tissues were gently dissociated by running through a 1-mL syringe attached to an 18-g needle. The dissociated cells were then allowed to attach to polylysine-coated coverslips for 24 h. Media consisting of high-glucose DMEM (Gibco), 10% (vol/vol) FCS, and 10 units/mL penicillin–streptomycin was replaced every 2–3 d. Schwann cells were confirmed by morphology and by staining with p75 and S100.

Immunocytochemistry. Sagittal sections of the trigeminal nerve were cut on a freezing microtome at a thickness of 8 μm and adhered to SuperFrost Plus Glass Slides (Fisher Scientific). Sections were then fixed using an ice-cold 2% (vol/vol) paraformaldehyde/PBS solution at 4 °C for 10 min. Sections were washed thoroughly with PBS and incubated at 37 °C for 2 h with CFTR antibodies. For verification of staining, two separate antibodies were used, M3A7 (Millipore 1:100) and clone 596 (Cystic Fibrosis Foundation; 1:200), on separate sections. Sections were then incubated with AlexaFluor-conjugated secondary antibodies (488 or 594) for 1 h at room temperature and washed. To visualize nuclei, a Hoechst stain (Invitrogen) was performed. For additional markers, the following were used: rabbit anti-β tubulin III (1:1,000; Abcam), FluoroMyelin (1:500; Invitrogen), rabbit anti S-100 (1:4,000; Dako), and goat anti-p75 (1:500; Neuromics). Sections were coverslipped using hard set mounting media (Vectashield) and imaged using an Olympus Fluoview FV1000 confocal microscope and UPLSAPO 60× oil lens. Identical microscope settings were used for $CFTR^{+/+}$ and $CFTR^{-/-}$ sections. Postcollection enhancements were done identically.

Whole-Cell Patch-Clamp Studies. An Axopatch 200B amplifier (Axon Instruments, Inc.) was used for voltage-clamping and current recording, and the pCLAMP software package (version 9.1; Axon Instruments, Inc.) was used for data acquisition and analysis. Holding voltage was −70 mV. Current recordings were lowpass-filtered at 500 Hz using an 8-pole Bessel filter (model 900; Frequency Devices, Inc.). The pipette (intracellular) solution contained (in mM): 140 *N*-methyl-D-glucamine, 10 tricine, 3 $MgCl_2$, 1 CsEGTA with 2 mM MgATP, and 2 μg/μL catalytic subunit of PKA from bovine heart (Calbiochem EMD Millipore), pH 7.3, with HCl. The bath (extracellular) solution contained (in mM): 140 *N*-methyl-D-glucamine, 10 tricine, 3 $MgCl_2$, and 5 $CaCl_2$, pH 7.3, with HCl. Experiments were performed at room temperature (24 °C).

Trigeminal Nerve Axon and Circumference Measurements. Whole trigeminal nerves were placed into Karnovsky's fixative for 48 h, sucrose-protected, and then sectioned. Cross-sections of the trigeminal nerve were cut at a thickness of 14 μm using a freezing microtome. Sections were stained using fluoromyelin (1:1,000; Invitrogen) and coverslipped using glycerol. Images were collected using an inverted two-photon microscope (Zeiss LSM 510 META). Multiple microscopic fields (~10–15) were taken from each nerve. Outer portions of the nerve bundle were preferentially targeted to ensure proper fixation. Using Image J, a grid was placed over each image, and one axon chosen randomly per each grid area was measured in sequential fashion until ~100 axons had been measured per image. The shortest axis was measured to correct for potential sectioning artifacts (58). Axons were marked using Image J software to ensure that duplication of axon measurements did not occur. Measurements were done by an observer blinded to genotype.

Trigeminal nerve circumference was measured using fine thread. Briefly, fine thread was tied around the trigeminal nerve at three equidistant points (encompassing the entire trigeminal nerve). The length was measured, and each point was averaged to generate one circumference measurement for each pig. Measurements were done by an observer blinded to genotype.

Electron Microscopy. The caudal portion of the trigeminal nerve was submerged in ice-cold Karnovsky's fixative for >48 h. A 1-mm cubed section was then cut, washed, and immersed in 2% (vol/vol) osmium tetroxide for 2 h. The cubed section was rinsed with increasing concentrations of ethanol and a final rinse in 100% propylene oxide. Following dehydration, cubes were placed in a 2:1 100% propylene oxide-Spurrs resin for 2 h followed by a 1:2 100% propylene oxide-Spurrs resin for 8 h. Samples were then infiltrated in three changes of 100% Spurrs resin for at least 2 h and polymerized for 24 h in a 60 °C oven. Tissue blocks were trimmed and sectioned at 80 nm for transmission electron microscopy and collected on gold grids. Poststaining of grids with uranyl acetate and lead citrate occurred before imaging on a JEOL 1230 TEM (JEOL USA Inc.) equipped with a Gatan 2k × 2k camera (Gatan Inc.).

Conduction Velocity Experiments. Conduction velocity experiments were performed using the sucrose gap method (59). Accordingly, the entire maxillary branch of the trigeminal nerve was quickly removed and immediately placed in artificial cerebral spinal fluid (aCSF) (in mM: 125 NaCl, 2.5 KCl, 1.25 NaH_2PO_4, 2 $CaCl_2$, 1.3 $MgSO_4$, 26 $NaHCO_3$, and 10 glucose, pH 7.4) bubbled with 95% O2 + 5% CO_2 gas mixture. Following a 2-h incubation period, the nerve was mounted in a specially designed chamber (University of Iowa Medical Instruments) modeled after Velumian and colleagues (59). The KCl compartments were perfused with a solution containing (in mM): 7.5 NaCl, 120 KCl, 1.25 Na_2HPO_4, 2 $CaCl_2$, 1.3 $MgSO_4$, 26 $NaHCO_3$, and 10 glucose, and the sucrose compartments were perfused with sucrose solution containing 305 mM sucrose. Both KCl and sucrose were isotonic to aCSF (305 mOsm). Stimuli were applied using an Anapulse Stimulator (model 302T; World Precision Instruments) and isolation unit (model 305; World Precision Instruments). Recording electrodes were connected to the headstage of a HS2A amplifier. The signals were filtered at 1 Khz and processed using Digidata 1200. Data were analyzed using clampfit software (version 9.2). Stimulation occurred for 10 μs in 1-s intervals. Conduction velocity was measured at stimulation that was 20% beyond that which gave the maximal response (as determined by amplitude) and calculated as latency to onset divided by distance between stimulating and recording electrodes (fixed distances in our chamber).

A portion of the sciatic nerve was removed that extended from the tip of the hip joint to the bifurcation point. The surrounding connective tissue was gently teased away, and membranes were removed. The sciatic nerves were then allowed to incubate for 2 h in bubbled aCSF. Identical procedures and methods used for the trigeminal nerve were used for conduction velocity experiments in the sciatic nerve.

Auditory Brainstem Evoked Potentials. Newborn pigs were anesthetized using ketamine (10–20 mg/kg) and xylazine (0.2–2.2 mg/kg). A s.c. reference electrode was placed immediately behind the test ear, a positive electrode was placed behind the contralateral ear, and a ground electrode was placed in the leg. Clicks were generated by a 12-bit digital-to-analog converter operating at 20,000 samples per second. Acoustic stimuli were presented at 80 db (normal hearing level) followed by decreasing stimulation (in 10-db increments). Simulation lasted 200 μs at a rate of 21.1 clicks per second and was delivered directly into the test ear through a Beyer model DT-40 earphone fitted with a custom earpiece. The earpiece allowed for insertion of the microphone just adjacent to the tympanic membrane. Stimulation at 70 db provided the clearest waveforms and was used for assessment of latencies. Auditory-brainstem-evoked-potential responses were performed on both ears, and averages were calculated per animal.

Statistical Analysis. Results are expressed as mean ± SEM or mean only. When only two groups were present, statistical significance was determined by $P \leq 0.05$, and differences were evaluated with an unpaired two-tailed *t* test. When three groups were present, a one-way ANOVA was performed. Planned comparisons using an unpaired two-tailed *t* test were made between $CFTR^{+/+}$ and $CFTR^{-/-}$ groups. Because each comparison tested a unique hypothesis, comparisons were performed irrespective of the outcome of the ANOVA (60). If the ANOVA was significant, post hoc tests were performed to determine whether $CFTR^{+/-}$ differed from $CFTR^{+/+}$. Statistical significance was determined by $P \leq 0.05$.

ACKNOWLEDGMENTS. We thank Ricky Bahner, Tania Rokhlina, Paula Ludwig, Alex Tucker, Theresa Mayhew, Martin Cassell, David Meyerholz, and Lynda S. Ostegaard for help and advice. This work was supported by the National Heart, Lung, and Blood Institute (HL91842 and T32HL007121-36) and the Cystic Fibrosis Foundation. M.J.W. is an Investigator of the Howard Hughes Medical Institute.

1. Welsh MJ, Ramsey BW, Accurso F, Cutting GR (2001) Cystic fibrosis. *The Metabolic and Molecular Basis of Inherited Disease*, eds Scriver CR, Beaudet AL, Sly WS, Valle D, Childs B, Vogelstein B (McGraw-Hill, New York), 8th Ed, pp 5121–5189.
2. Quinton PM (1999) Physiological basis of cystic fibrosis: A historical perspective. *Physiol Rev* 79(1):Suppl):S3–S22.
3. Rowe SM, Miller S, Sorscher EJ (2005) Cystic fibrosis. *N Engl J Med* 352(19):1992–2001.
4. El-Salem K, Aburahma S, Rawashdeh M (2010) Peripheral nerve dysfunction in patients with cystic fibrosis. *J Clin Neurophysiol* 27(3):216–218.
5. O'Riordan JI, Hayes J, Fitzgerald MX, Redmond J (1995) Peripheral nerve dysfunction in adult patients with cystic fibrosis. *Ir J Med Sci* 164(3):207–208.
6. Heinz-Erian P, Dey RD, Flux M, Said SI (1985) Deficient vasoactive intestinal peptide innervation in the sweat glands of cystic fibrosis patients. *Science* 229(4720):1407–1408.
7. Bentur L, et al. (2006) Impaired gastric myoelectrical activity in patients with cystic fibrosis. *J Cyst Fibros* 5(3):187–191.
8. Davis PB, Kaliner M (1983) Autonomic nervous system abnormalities in cystic fibrosis. *J Chronic Dis* 36(3):269–278.

9. Davis PB, Shelhamer JR, Kaliner M (1980) Abnormal adrenergic and cholinergic sensitivity in cystic fibrosis. *N Engl J Med* 302(26):1453–1456.
10. Vaisman N, Tabachnik E, Shahar E, Gilai A (1996) Impaired brainstem auditory evoked potentials in patients with cystic fibrosis. *Dev Med Child Neurol* 38(1):59–64.
11. Staley K, Iragui VJ (1991) Somatosensory dysfunction in cystic fibrosis. *Eur Neurol* 31 (2):77–81.
12. Bureau MA, Lupien L, Bégin R (1981) Neural drive and ventilatory strategy of breathing in normal children, and in patients with cystic fibrosis and asthma. *Pediatrics* 68(2):187–194.
13. Gild R, Clay CD, Morey S (2010) Aquagenic wrinkling of the palms in cystic fibrosis and the cystic fibrosis carrier state: A case–control study. *Br J Dermatol* 163(5):1082–1084.
14. Patel AJ, Raol VH, Jea A (2011) Rare association between cystic fibrosis, Chiari I malformation, and hydrocephalus in a baby: A case report and review of the literature. *J Med Case Reports* 5:366.
15. Liu GJ, Kalous A, Werry EL, Bennett MR (2006) Purine release from spinal cord microglia after elevation of calcium by glutamate. *Mol Pharmacol* 70(3):851–859.
16. Mulberg AE, et al. (1994) Cystic fibrosis transmembrane conductance regulator protein expression in brain. *Neuroreport* 5(13):1684–1688.
17. McGrath SA, Basu A, Zeitlin PL (1993) Cystic fibrosis gene and protein expression during fetal lung development. *Am J Respir Cell Mol Biol* 8(2):201–208.
18. Niu N, Zhang J, Guo Y, Yang C, Gu J (2009) Cystic fibrosis transmembrane conductance regulator expression in human spinal and sympathetic ganglia. *Lab Invest* 89(6): 636–644.
19. Davis PB (1984) Autonomic and airway reactivity in obligate heterozygotes for cystic fibrosis. *Am Rev Respir Dis* 129(6):911–914.
20. Rogers CS, et al. (2008) Production of CFTR null and ΔF508 heterozygous pigs by AAV-mediated gene targeting and somatic cell nuclear transfer. *J Clin Invest* 118(4): 1571–1577.
21. Rogers CS, et al. (2008) Disruption of the CFTR gene produces a model of cystic fibrosis in newborn pigs. *Science* 321(5897):1837–1841.
22. Stoltz DA, et al. (2010) Cystic fibrosis pigs develop lung disease and exhibit defective bacterial eradication at birth. *Sci Transl Med* 2(29):29ra31.
23. Muanprasat C, et al. (2004) Discovery of glycine hydrazide pore-occluding CFTR inhibitors: Mechanism, structure-activity analysis, and in vivo efficacy. *J Gen Physiol* 124 (2):125–137.
24. Fabrizi GM, et al. (2000) Focally folded myelin in Charcot–Marie–Tooth neuropathy type 1B with Ser49Leu in the myelin protein zero. *Acta Neuropathol* 100(3):299–304.
25. Gambardella A, et al. (1998) Genetic heterogeneity in autosomal recessive hereditary motor and sensory neuropathy with focally folded myelin sheaths (CMT4B). *Neurology* 50(3):799–801.
26. Tersar K, et al. (2007) Mtmr13/Sbf2-deficient mice: An animal model for CMT4B2. *Hum Mol Genet* 16(24):2991–3001.
27. Quattrone A, et al. (1996) Autosomal recessive hereditary motor and sensory neuropathy with focally folded myelin sheaths: Clinical, electrophysiologic, and genetic aspects of a large family. *Neurology* 46(5):1318–1324.
28. Patzko A, Shy ME (2012) Charcot–Marie–Tooth disease and related genetic neuropathies. *Continuum (Minneap Minn)* 18(1):39–59.
29. Maeda MH, et al. (2012) Increased gene dosage of myelin protein zero causes Charcot–Marie–Tooth disease. *Ann Neurol* 71(1):84–92.
30. Fratta P, et al. (2011) P0S63del impedes the arrival of wild-type P0 glycoprotein to myelin in CMT1B mice. *Hum Mol Genet* 20(11):2081–2090.
31. Rünker AE, et al. (2004) Pathology of a mouse mutation in peripheral myelin protein P0 is characteristic of a severe and early onset form of human Charcot–Marie–Tooth type 1B disorder. *J Cell Biol* 165(4):565–573.
32. Nobbio L, et al. (2009) P2X7-mediated increased intracellular calcium causes functional derangement in Schwann cells from rats with CMT1A neuropathy. *J Biol Chem* 284(34):23146–23158.
33. Wrabetz L, et al. (2000) P(0) glycoprotein overexpression causes congenital hypomyelination of peripheral nerves. *J Cell Biol* 148(5):1021–1034.
34. Eberhard DA, Brown MD, VandenBerg SR (1994) Alterations of annexin expression in pathological neuronal and glial reactions. Immunohistochemical localization of annexins I, II (p36 and p11 subunits), IV, and VI in the human hippocampus. *Am J Pathol* 145(3):640–649.
35. Shames I, Fraser A, Colby J, Orfali W, Snipes GJ (2003) Phenotypic differences between peripheral myelin protein-22 (PMP22) and myelin protein zero (P0) mutations associated with Charcot–Marie–Tooth-related diseases. *J Neuropathol Exp Neurol* 62 (7):751–764.
36. Chapon F, Latour P, Diraison P, Schaeffer S, Vandenberghe A (1999) Axonal phenotype of Charcot–Marie–Tooth disease associated with a mutation in the myelin protein zero gene. *J Neurol Neurosurg Psychiatry* 66(6):779–782.
37. Starr A, Picton TW, Sininger Y, Hood LJ, Berlin CI (1996) Auditory neuropathy. *Brain* 119(Pt 3):741–753.
38. Høyer H, Braathen GJ, Eek AK, Skjelbred CF, Russell MB (2011) Charcot–Marie–Tooth caused by a copy number variation in myelin protein zero. *Eur J Med Genet* 54(6): e580–e583.
39. Niemann S, Sereda MW, Suter U, Griffiths IR, Nave KA (2000) Uncoupling of myelin assembly and Schwann cell differentiation by transgenic overexpression of peripheral myelin protein 22. *J Neurosci* 20(11):4120–4128.
40. Hattori N, et al.; Study Group for Hereditary Neuropathy in Japan (2003) Demyelinating and axonal features of Charcot–Marie–Tooth disease with mutations of myelin-related proteins (PMP22, MPZ and Cx32): A clinicopathological study of 205 Japanese patients. *Brain* 126(Pt 1):134–151.
41. Misu K, et al. (2000) An axonal form of Charcot–Marie–Tooth disease showing distinctive features in association with mutations in the peripheral myelin protein zero gene (Thr124Met or Asp75Val). *J Neurol Neurosurg Psychiatry* 69(6):806–811.
42. Cynamon HA, Milov DE, Valenstein E, Wagner M (1988) Effect of vitamin E deficiency on neurologic function in patients with cystic fibrosis. *J Pediatr* 113(4):637–640.
43. Ramirez JD, Barnes PR, Mills KR, Bennett DL (2012) Intermediate Charcot–Marie–Tooth disease due to a novel Trp101Stop myelin protein zero mutation associated with debilitating neuropathic pain. *Pain* 153(8):1763–1768.
44. Mastaglia FL, et al. (1999) Novel mutation in the myelin protein zero gene in a family with intermediate hereditary motor and sensory neuropathy. *J Neurol Neurosurg Psychiatry* 67(2):174–179.
45. Kraus A, et al. (2010) Calnexin deficiency leads to dysmyelination. *J Biol Chem* 285(24): 18928–18938.
46. Wilkins A, et al. (2010) Slowly progressive axonal degeneration in a rat model of chronic, nonimmune-mediated demyelination. *J Neuropathol Exp Neurol* 69(12): 1256–1269.
47. Wilson GF, Chiu SY (1993) Mitogenic factors regulate ion channels in Schwann cells cultured from newborn rat sciatic nerve. *J Physiol* 470:501–520.
48. Byun N, Delpire E (2007) Axonal and periaxonal swelling precede peripheral neurodegeneration in KCC3 knockout mice. *Neurobiol Dis* 28(1):39–51.
49. Lind NM, et al. (2007) The use of pigs in neuroscience: Modeling brain disorders. *Neurosci Biobehav Rev* 31(5):728–751.
50. Borovikova LV, et al. (2000) Vagus nerve stimulation attenuates the systemic inflammatory response to endotoxin. *Nature* 405(6785):458–462.
51. Chmiel JF, Konstan MW (2007) Inflammation and anti-inflammatory therapies for cystic fibrosis. *Clin Chest Med* 28(2):331–346.
52. Wine JJ, Joo NS (2004) Submucosal glands and airway defense. *Proc Am Thorac Soc* 1 (1):47–53.
53. Burns AJ, Roberts RR, Bornstein JC, Young HM (2009) Development of the enteric nervous system and its role in intestinal motility during fetal and early postnatal stages. *Semin Pediatr Surg* 18(4):196–205.
54. De Giorgio R, et al. (2004) New insights into human enteric neuropathies. *Neurogastroenterol Motil* 16(Suppl 1):143–147.
55. Davidson AC, Harrison K, Steinfort CL, Geddes DM (1987) Distal intestinal obstruction syndrome in cystic fibrosis treated by oral intestinal lavage, and a case of recurrent obstruction despite normal pancreatic function. *Thorax* 42(7):538–541.
56. Rogan MP, et al. (2010) Pigs and humans with cystic fibrosis have reduced insulin-like growth factor 1 (IGF1) levels at birth. *Proc Natl Acad Sci USA* 107(47):20571–20575.
57. Ullian EM, Harris BT, Wu A, Chan JR, Barres BA (2004) Schwann cells and astrocytes induce synapse formation by spinal motor neurons in culture. *Mol Cell Neurosci* 25(2): 241–251.
58. Dubowitz V, Lane R, Sewry CA (2007) *Muscle Biopsy: A Practical Approach* (Saunders Elsevier, Philadelphia), 3rd Ed.
59. Velumian AA, Wan Y, Samoilova M, Fehlings MG (2010) Modular double sucrose gap apparatus for improved recording of compound action potentials from rat and mouse spinal cord white matter preparations. *J Neurosci Methods* 187(1):33–40.
60. Ruxton GD, Beauchamp GK (2008) Time for some a priori thinking about post hoc testing. *Behav Ecol* 19(3):690–693.